Melting-induced crustal production helps plate tectonics on Earth-like planets

Diogo L. Lourenço *, Antoine Rozel, Paul J. Tackley

Institute of Geophysics, Department of Earth Sciences, ETH Zurich, Sonneggstrasse 5, CH-8092 Zurich, Switzerland

A B S T R A C T

Within our Solar System, Earth is the only planet to be in a mobile-lid regime. It is generally accepted that the other terrestrial planets are currently in a stagnant-lid regime, with the possible exception of Venus that may be in an episodic-lid regime. In this study, we use numerical simulations to address the question of whether melting-induced crustal production changes the critical yield stress needed to obtain mobile-lid behaviour (plate tectonics). Our results show that melting-induced crustal production strongly influences plate tectonics on Earth-like planets by strongly enhancing the mobility of the lid, replacing a stagnant lid with an episodic lid, or greatly extending the time in which a smoothly evolving mobile lid is present in a planet. Finally, we show that our results are consistent with analytically predicted critical yield stress obtained with boundary layer theory, whether melting-induced crustal production is considered or not.

© 2016 The Authors. Published by Elsevier B.V. This is an open access article under the CC BY-NC-ND license (http://creativecommons.org/licenses/by-nc-nd/4.0/).

1. Introduction

Although the effects of melting and crustal production for planetary evolution and dynamics are acknowledged as being very important (Stevenson, 1990; Xie and Tackley, 2004; Davies, 2007; Ogawa and Yanagisawa, 2011; Nakagawa and Tackley, 2012), their effects on the mobility of the lithosphere are poorly understood. The different convection regimes and the general effects of melting are reviewed next in this section. In this article, for the purpose of a better readability, we will use the acronym "MCP" to represent "melting-induced crustal production".

1.1. Lid regime

In the Solar System, Earth is the only planet to be in a mobile-lid regime (Tackley, 2000; Stein et al., 2004), whilst it is generally accepted that all the other terrestrial planets are currently in a stagnant-lid regime (Solomatov, 1995), showing little or no surface motion. A transitional regime between these two, showing episodic overturns of an unstable stagnant lid, has been reported and might apply to Venus (Moresi and Solomatov, 1998; Rozel, 2012; Armann and Tackley, 2012).

It has been shown that a convection regime similar to plate tectonics can be modelled using strongly temperature-dependent viscosity and plastic yielding (Fowler, 1993; Moresi and Solomatov, 1998; Tackley, 2000; Stein et al., 2004). In these models, a maximal stress is imposed in the lithosphere. If stresses exceed this value, named the yield stress, the viscosity is decreased to bring the stresses back to the critical value. This is sufficient to break the lithosphere into "plates". However, the exact value of the stresses reached in the lithosphere strongly depends on the rheology (Fowler, 1985; Solomatov, 1995; Reese et al., 1998; Solomatov, 2004), and also on the surface boundary condition used in numerical simulations (Crameri et al., 2012). The critical yield stress necessary to obtain mobile-lid (plate-like) behaviour in numerical simulations is much lower than what is expected from laboratory rock deformation experiments (Kohlstedt et al., 1995). An explanation for this may be related to the presence of water in nature (Regenauer-Lieb et al., 2001; Dymkova and Gerya, 2013).

Numerical models typically focus on purely thermal convection, whereas compositional variations in the lithosphere can alter the stress state, simply by thickening the lithosphere or by providing lateral density anomalies that in turn produce additional stresses, greatly influencing the likelihood of plate tectonics. For example, Rolf and Tackley (2011) showed that the addition of a continent can reduce the critical yield stress for mobile-lid behaviour by a factor of around two, while Armann and Tackley (2012) found that bursts of crustal production caused by partial melting may trigger lithospheric overturn events, suggesting that melting may also play an important role in facilitating plate tectonics. Complicating matters is the finding that the final state of the system (stag-

* Corresponding author.
E-mail address: diogo.lourenco@erdw.ethz.ch (D.L. Lourenço).

nant or mobile lid) can depend on initial conditions (Tackley, 2000; Weller and Lenardic, 2012; Lenardic and Crowley, 2012).

1.2. Melting and crustal production

Melting plays a major role in the evolution of planets' interiors, both during their formation and during their subsequent long-term evolution over billions of years (Stevenson, 1990; Nakagawa and Tackley, 2012). On present-day Earth, melting mainly occurs in the shallow mantle below the tectonic plates (McKenzie and Bickle, 1988), and may also occur in deeper regions of the upper mantle and above the core–mantle boundary (CMB) (Williams and Garnero, 1996). The surface expression of melting is volcanism, which on present-day Earth occurs mostly as the formation of oceanic crust at mid-ocean spreading centres (Schubert et al., 2001).

Partial melting causes differentiation when crust is produced at mid-ocean ridges because the major element composition of the melt is different from that of the source rock, thus leaving a depleted residue. Trace elements are generally incompatible and enter the melt phase (Hofmann, 1997). Some of them contain heat-producing isotopes, which contribute to around 50% of the present-day heat loss from the interior (Davies, 2007). Also, partial melting modulates heat loss from the interior by transporting heat from the interior to the surface, where it erupts, solidifies and cools. The advected heat cools the planet, but at the same time, melting absorbs latent heat locally, which lessens the maximum mantle temperature.

Another effect of mantle melting is that it dehydrates and stiffens the shallow part of the mantle (Hirth and Kohlstedt, 1996). It introduces viscosity and compositional stratifications in the shallow mantle, because viscosity increases with the loss of hydrogen upon melting (Faul and Jackson, 2007; Korenaga and Karato, 2008). Also, the presence of melt along grain edges influences the deformation rate of grains, and therefore the viscosity (Zimmerman and Kohlstedt, 2004; Scott and Kohlstedt, 2006). While these effects may be significant, we do not consider them in this work.

Therefore, melting has a major role in the long-term evolution of rocky planets, enhancing heat loss, causing chemical differentiation of the interior and influencing geochemical signatures. Although it has been taken into account in some thermal evolution studies, its effect on plate tectonics has never been systematically studied.

1.3. This study

In this article, we present a set of 2D spherical annulus simulations of mantle convection (Hernlund and Tackley, 2008) considering MCP. We focus on the question of whether MCP changes the critical yield stress required to obtain mobile-lid behaviour as a function of governing parameters, particularly the reference viscosity. We first describe our model in section 2. In section 3 we present our results, which are discussed in section 4. Finally, in section 5 we present the conclusions of this study.

2. Numerical model and physical model

The numerical model used here is based on the one described by Armann and Tackley (2012) and Tackley et al. (2013), although with parameters adjusted to the case of the Earth. The model incorporates realistic parameter values and physics descriptive of planet Earth, and thus includes compressibility, phase transitions, pressure–temperature-dependence of viscosity, time-dependent internal and basal heating and plasticity. Diffusion creep, with the assumption of homogeneous grain size, is the assumed deformation mechanism. The values used for the standard physical parameters are given in Table 1. Throughout our study we varied the

Table 1

Physical properties. (UM = Upper Mantle (dry olivine); PV = Perovskite; PPV = Post-Perovskite; Act. en. stands for Activation energy, Act. vol. for Activation volume.)

Property	Symbol	Value	Units
Surface temperature	T_{surf}	300	K
Init. potential temp.	T_{P0}	1600	K
Specific heat capacity	C_p	1200	J/kg/K
Gas constant	R	8.3145	J/K/mol
Latent heat of melting	L	600	kJ/kg
Internal heating rate	H	$18.77 \cdot 10^{-12}$	W/kg
Half-life	t_{half}	2.43	Ga
Act. en. - UM	E_{ol}	300	kJ/mol
Act. vol. - UM	V_{ol}	5.00	cm^3/mol
p_{decay} - UM	p_{decay_ol}	∞	GPa
Act. en. - PV	E_{pv}	370	kJ/mol
Act. vol. - PV	V_{pv}	3.65	cm^3/mol
p_{decay} - PV	p_{decay_pv}	200	GPa
Act. en. - PPV	E_{ppv}	162	kJ/mol
Act. vol. - PPV	V_{ppv}	1.40	cm^{3}mol
p_{decay} - PPV	p_{decay_ppv}	1610	GPa
Thermal expansivity	α	$5 \cdot 10^{-5}$	K^{-1}
Density	ρ	3300	kg/m^3
Gravity	g	9.81	m/s^2
Mantle thickness	h	2890	km
Thermal diffusivity	κ	$7.6 \cdot 10^{-7}$	m^2/s
mid-UM pressure	P_{UM}	30	GPa
Density difference	$\Delta\rho$	200	kg/m^3
Phase trans. eclogite	D_{ecl}	60	km

reference viscosity and the yield stress in the model, as well as whether or not MCP is included. Within this framework, the effect of MCP was systematically tested.

2.1. Rheology

In our models, the viscous deformation mechanism is diffusion creep, which is assumed to follow a temperature- and pressure-dependent Arrhenius law:

$$\eta_{diff}(T, p) = \eta_0 \exp\left(\frac{E + pV}{RT} - \frac{E}{RT_0}\right), \qquad (1)$$

where η_0 is the reference viscosity at zero pressure and reference temperature T_0 (= 1600 K), E is the activation energy, p is the pressure, V is the activation volume, T is the absolute temperature and R is the gas constant. Different values for E and V are used for the upper and lower mantle (Karato and Wu, 1993; Yamazaki and Karato, 2001) and can be seen in Table 1. The activation volume decreases with increasing pressure according to the formula:

$$V(p) = V_0 \exp\left(-\frac{p}{p_{decay}}\right). \qquad (2)$$

p_{decay} is given in Table 1. A viscosity jump of 10 is imposed at the transition between the upper and lower mantle (Čížková et al., 2012 and references therein). A second viscosity jump of 10^{-3} (compared with the above material) is imposed at the transition to post-perovskite at lowermost mantle depths, as suggested by mineral physics experiments and theoretical calculations (Ammann et al., 2010; Hunt et al., 2009). The reference viscosity η_0 is varied in our simulations, ranging from $5 \cdot 10^{19}$ Pa·s to 10^{21} Pa·s.

In order to obtain plate-like behaviour, plastic yielding is employed (Moresi and Solomatov, 1998; Tackley, 2000). It is assumed that the material deforms plastically after reaching a yield stress:

$$\tau_y = \tau_{duct} + \tau'_{duct} \, p, \qquad (3)$$

where τ_{duct} is the ductile yield stress and τ'_{duct} is the vertical gradient of the ductile yield stress. In practice, this last parameter prevents yielding in the deep mantle. The parameter with the greatest influence in the previous equation is τ_{duct}, and is therefore

Table 2
Phase change parameters. ρ_{surf} stands for surface density, $\Delta\rho_{\text{pc}}$ for the density jump across a phase transition and γ for the Clapeyron slope.

Depth (km)	Temperature (K)	$\Delta\rho_{\text{pc}}$ (kg/m^3)	γ (MPa/K)
	Olivine ($\rho_{\text{surf}} = 3240$ kg/m^3)		
410	1600	180	+2.5
660	1900	400	−2.5
2740	2300	61.6	+10.0
	Pyroxene–garnet ($\rho_{\text{surf}} = 3080$ kg/m^3)		
60	1000	350	0
400	1600	150	+1.0
720	1900	400	+1.0
2740	2300	61.6	+10.0

the second parameter that we vary in our study. We used values between 20 and 300 MPa, in intervals of 20 MPa.

Finally, the effective viscosity is the harmonic average of the two contributions from equations (1) and (3):

$$\eta_{\text{eff}} = \left(\frac{1}{\eta_{\text{diff}}} + \frac{2\dot{\varepsilon}}{\tau_{\text{y}}} \right)^{-1}, \qquad (4)$$

where $\dot{\varepsilon}$ is the second invariant of the strain rate tensor. The viscosity is not dependent on melt fraction or composition.

2.2. Phase changes, composition, melting-induced crustal production

A parameterisation based on mineral physics data (e.g. Irifune and Ringwood, 1993; Ono et al., 2001) is included in the model, dividing minerals into the olivine and pyroxene–garnet systems, which undergo different solid–solid phase transitions, as used in previous studies (Xie and Tackley, 2004; Nakagawa and Tackley, 2012). Parameter values are given in Table 2, where $\Delta\rho_{\text{pc}}$ is the density jump across a phase transition and γ is the Clapeyron slope. The phase transition to post-perovskite at lowermost mantle depths is included (e.g. Tackley et al., 2013). The mixture of minerals depends on the chemical composition, which varies between two end-members: basalt (pure pyroxene–garnet) and harzburgite (75% olivine). As in previous studies (e.g. Xie and Tackley, 2004; Nakagawa et al., 2010), changes in composition arise from melt-induced differentiation. At each time step, the temperature in each cell is compared to the solidus temperature as used by Nakagawa and Tackley (2004), which is a function that fits experimental data by Herzberg et al. (2000) in the upper mantle and by Zerr et al. (1998) in the lower mantle. If the temperature in a specific cell exceeds the solidus then enough melt is generated in order to bring the temperature back to solidus, leaving a more depleted residue behind depending on the degree of melt extracted. Melting can only occur if the material is not completely depleted. Another assumption made is that the percolation of melt through the solid is much faster than convection (Condomines et al., 1988) and thus shallow melt is instantly removed and deposited at the surface to form oceanic crust with the surface temperature. Segregation of heat-producing elements into the crust is not included in our models.

2.3. Boundary conditions and solution method

We use a spherical annulus geometry (Hernlund and Tackley, 2008) employing free slip boundary conditions at the surface and core–mantle boundary to address the thermochemical evolution of Earth over 4.5 billion years. The temperature at the surface is fixed to 300 K. The initial potential temperature is 1600 K. Core cooling is assumed, based on the works by Buffett et al. (1992) and Buffett et al. (1996). Details on the parameterisation used for core cooling can be found in Nakagawa and Tackley (2004).

We solve the equations for compressible anelastic Stokes flow with infinite Prandtl number, using the code StagYY (Tackley, 2008). This uses a finite-volume scheme for advection of temperature, a multigrid solver to obtain a velocity–pressure solution at each time-step, tracers to track composition, and the treatment of partial melting and crustal formation described above. The used computational resolution is composed by 256×64 cells, in which one million tracers are advected. We performed resolution tests with up to four times the number of points in each direction for selected cases and we did not observe a significant change in the dynamics of our models. For more details on the code StagYY, the reader is referred to Tackley (2008).

3. Results

3.1. Convective regimes

The results obtained are summarised in Fig. 1, which shows the convective regime (mobile, episodic or stagnant lid) for all the simulations, as a function of the reference viscosity and yield stress, based on the mobility of the surface. For each yield stress and reference viscosity we ran two simulations: one without MCP, i.e. purely thermal convection (Fig. 1(A) where the mobility is shown in black numbers) and one with MCP (Fig. 1(B) where the mobility is shown in red numbers). We compute the mobility as the percentage of time in the evolution of the planet in which the surface velocity is higher than 1 cm/yr. This criterion is somewhat arbitrary, but reasonable. Other values were tested, but it was found that the effect on the regime boundaries is negligible, except for high reference viscosities, for which the typical surface velocities in the mobile-lid regime decrease towards the chosen threshold. Even so, the effect is small.

If the mobility is 0% then there is no significant surface motion during the planet's evolution and therefore the convective regime in the model is stagnant lid. If the mobility is larger than 60%, we assume that the planet had enough surface motion during a significant part of its evolution, so that the convective regime can be classified as mobile lid. Between 1–59% mobility we classify the convective regime as episodic lid. The expression of this episodicity is diverse and we will address this matter later. The value of mobility we have chosen for the regime boundaries is again somewhat arbitrary, however it doesn't make much difference because the value of mobility changes rapidly across regime boundaries.

A stagnant lid is obtained at high yield stresses because naturally developing convective stresses remain lower than the yield stress. The mobile lid regime is obtained at low yield stresses, where plasticity is dominant in the lithosphere and a stagnant lid can never form. For intermediate yield stresses, an episodic lid is obtained for the cases with MCP, while subduction stops around 1–2 Gyrs for purely thermal cases (early-mobility regime). Black solid lines represent the regime boundaries for simulations without MCP in Fig. 1(A), while red solid lines represent the regime boundaries for simulations with MCP in Fig. 1(B).

Looking at the results without MCP in Fig. 1(A), we see a general trend where as the reference viscosity increases, the transition from mobile lid to early-mobility is shifted towards lower yield stress values and the transition from early-mobility to stagnant lid is shifted to higher yield stress values. This results in a wider window where an early-mobility behaviour is obtained with increasing reference viscosity.

When MCP is considered (Fig. 1(B)), the general trend of the transition from mobile-, to episodic-, to stagnant-lid regime, for increasing yield stresses (and the same reference viscosity) is the same (see the red lines). However, important changes can be ob-
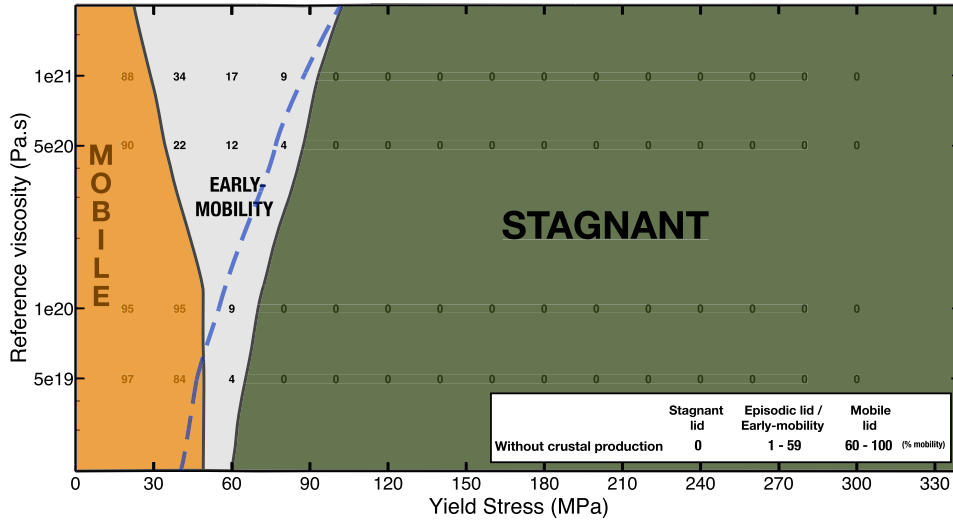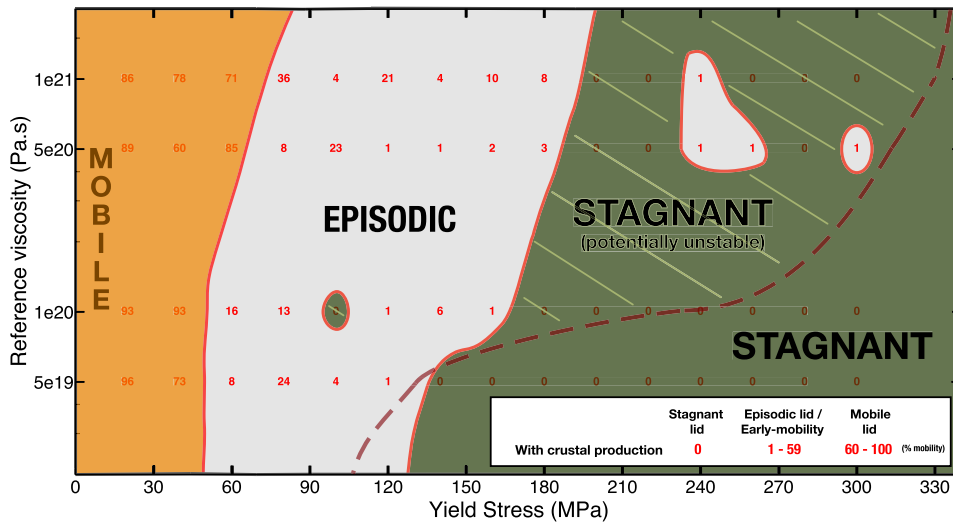
Fig. 1. Regime diagram in the parameter space of yield strength and reference viscosity for cases: (A) without considering MCP, and (B) considering MCP. Each number inside the diagrams represents one computation, and its colour indicates whether MCP is considered or not: (black) without MCP, (red) with MCP. The value represents the mobility, i.e. the percentage of time in which the surface velocity in the model is larger than 1 cm/yr. In (A), the black lines separate different regimes according to the numerical results, while the blue thick dashed line represents our analytically predicted transition from cases with some mobility to a stagnant-lid regime. In (B), the red lines separate different regimes according to the numerical results, while the red thick dashed line represents our analytically predicted transitions from cases with some mobility to a stagnant-lid regime.

served. As before, the transition from an episodic to a stagnant lid happens at higher yield stresses for higher reference viscosity values. However, this transition is shifted to larger yield stress values by an amount that can range from 60 MPa for a reference viscosity of $5 \cdot 10^{19}$ Pa·s to 220 MPa for a reference viscosity of $5 \cdot 10^{20}$ Pa·s. This means that the parameter interval in which the system has as a final state an episodic lid regime is wider. Additionally, the transition from an episodic to a stagnant lid is not continuous. For example, for a reference viscosity of 10^{21} Pa·s and a yield stress of 220 MPa there is no resurfacing, but for the same reference viscosity and a higher yield stress, 240 MPa, there is a transition from stagnant to episodic lid due to the effects of MCP. Also, it is possible to see that for higher reference viscosities and smaller yield stresses there is a transition from episodic to a mobile lid, which we name a transition from early-mobility to mobile lid. We will address these two last results in the discussion section. The main point here is that the results consistently show an increase in mobility as the result of MCP.

Fig. 2 shows two simulations with the same reference viscosity, 10^{21} Pa·s and the same yield stress, 100 MPa, differing in the use or not of MCP. For the case without MCP (Fig. 2(A)), we have a stagnant-lid regime case with the interior temperature increasing with time. However, for the case with MCP (Fig. 2(B)) an episodic-lid regime case with overturns of an unstable stagnant lid is obtained. The mobility of the lid helps to buffer the interior temperatures of the planet. One overturn of the lid is shown in Fig. 2(C) around 2.3 billion years after the beginning of the evolution of the planet. It can be seen that the timescale for such an event is on the order of 20–25 million years.

3.2. Surface velocity and average mantle temperature

In order to better understand the regime transitions between different models and throughout the evolution of our simulations, the surface velocities and average mantle temperatures for all the cases are plotted as a function of time in Fig. 3. Here, the time-
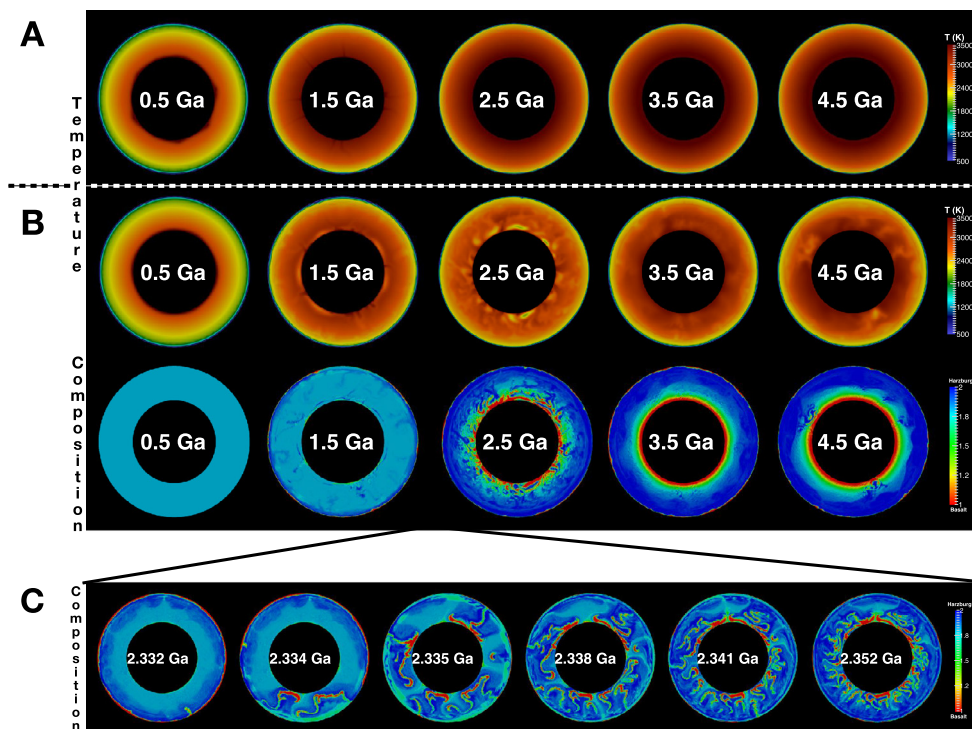
Fig. 2. Time evolution of the temperature field for the case with reference viscosity of 10^{21} Pa·s and yield stress of 100 MPa, for (A) stagnant lid case without MCP and (B) episodic lid case with MCP, plus compositional field for this case. Composition ranges from 1 (basalt) to 2 (harzburgite). (C) shows a temporal zoom-in of a global overturn event.

dependence of surface velocities can be clearly seen, while in Fig. 1 the values were averaged out.

For each reference viscosity and yield strength, two cases are presented, one with MCP (red line) and one without MCP (black line). We can clearly see the transitions between different convective regimes and also how cases with MCP have a higher mobility. In the stagnant-lid regime, surface velocities are negligible and large average mantle temperatures are reached as the planet heats up with time. The mobile-lid regime is characterised by mostly non-negligible surface velocities and low mantle temperatures. One can observe that the surface velocities strongly depend on the reference viscosity used, which is consistent with scaling laws based on boundary layer theory such as $v \propto \eta (T_i)^{-2/3}$ (Schubert et al., 2001), where $\eta (T_i)$ is the effective viscosity based on the internal temperature T_i.

An interesting observation is that different regimes are observed between mobile- and stagnant-lid regimes for cases with and without MCP. With MCP we observe bursts of mobilisation of the lid, i.e. fast overturns of a stagnant lid. For the case without MCP, a stopping of plate tectonics is observed after some time (that is why we call this regime early-mobility). This can again be understood using boundary layer theory, which also provides a scaling for the stresses: $\tau \propto \eta (T_i)^{1/3}$. Comparing Fig. 3(A) and Fig. 3(B), we can see that a mobile lid tends to quickly decrease the mantle temperature, thus increasing the viscosity, which results in stresses large enough to keep the lid mobile. In the early-mobility regime, the yield stress is too high to maintain the mobile-lid regime throughout all the evolution of the simulation: large yield stresses allow only a partial initial resurfacing, which does not cool the deep mantle enough to maintain high stresses. Even for lower yield stresses, for which a full resurfacing occurs leading to a longer mobile-lid regime, the cooling of the mantle is not enough and eventually the mantle heats up and plate tectonics is shut off. This effect is more important for higher reference viscosities because the time-dependence of viscosity is more influential due to the fact that as the mantle convects more slowly, the temperature

and viscosity take longer to reach an equilibrium state. This explains why the transition from a mobile lid to an early-mobility regime occurs for smaller yield stresses as the reference viscosity increases.

Finally, the transition from an early-mobility- to a stagnant-lid regime in the cases without MCP (purely thermal convection) occurs for higher yield strengths for higher reference viscosities. We will show that this is an expected behaviour predicted by classical boundary layer theory, in the discussion section.

4. Discussion

As shown in the previous section, the main effect of MCP is to increase the mobility of the lid by facilitating the breaking of a stagnant lid and replacing it with an episodic lid, or by notably extending the time in the evolution of the planet during which a smoothly evolving mobile lid is present. In this section we show that this increase of mobility is due to variations of lithosphere stresses owing to internal activity. We first look at internal temperatures, lid thicknesses and eruption rates of the models. Then we show that it is possible to analytically predict the increase of critical yield stress due to MCP.
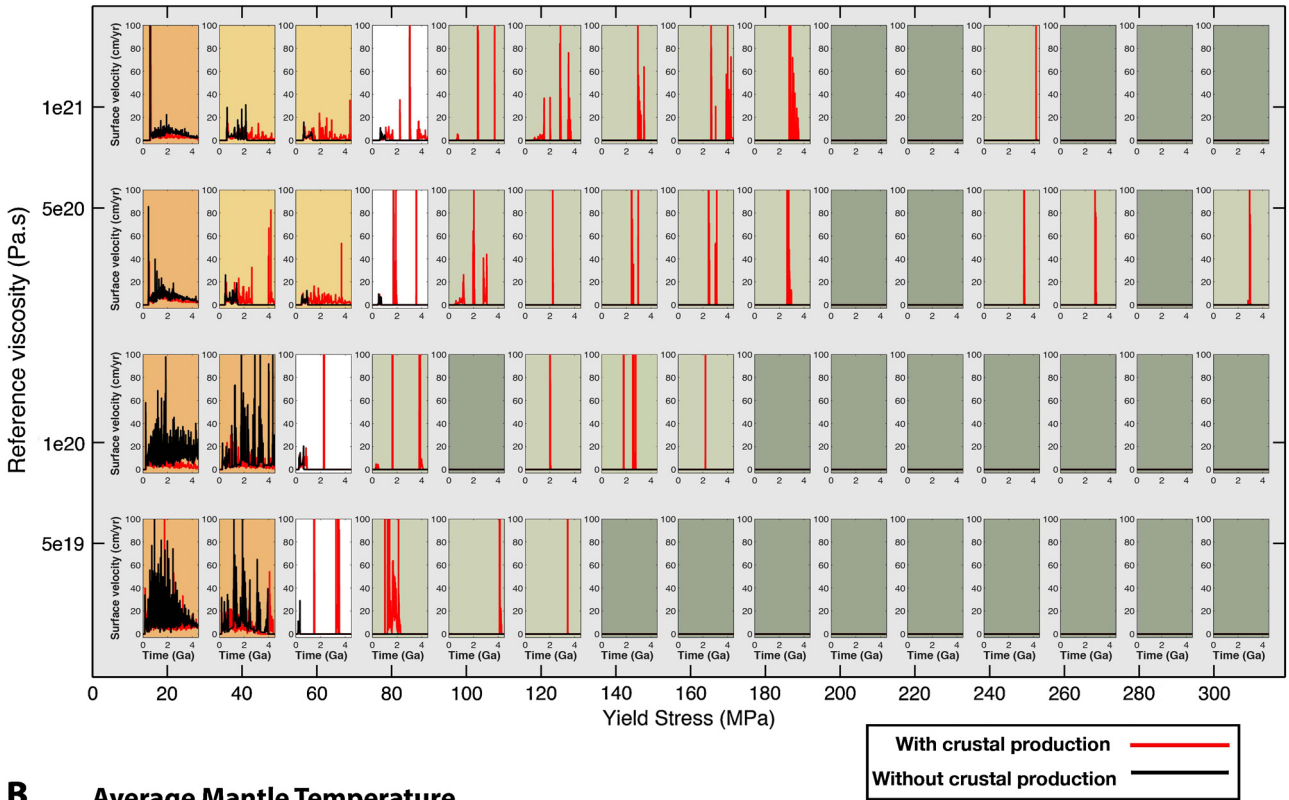
The effects of a different initial potential temperature in the mobility of the lid were examined and are presented in Supplementary material. In short, it was found that the effect of MCP on greatly changing regime boundaries is robust regardless of initial temperature, but the exact evolution depends somewhat on initial temperature, particularly earlier in the planet's history.

4.1. Effects of MCP

4.1.1. Lid thickness

Fig. 4(A) shows the lid thickness as a function of the yield stress for the different reference viscosities and considering or not MCP. The shown lid thickness values are an average over the last half
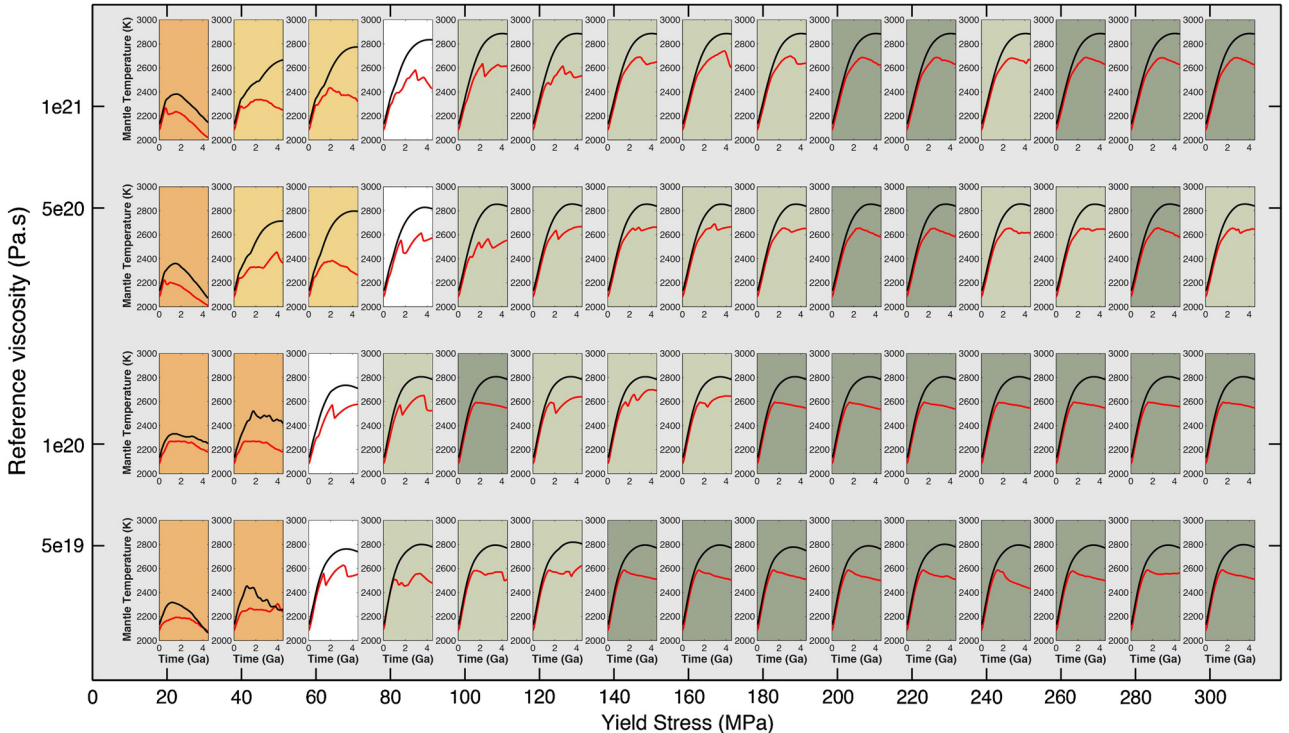
Fig. 3. (A) Surface velocity and (B) average mantle temperature as a function of time for all numerical simulations in the parameter space of yield stress and reference viscosity. For each reference viscosity and yield stress, two cases are represented, one with MCP (red line) and one without MCP (black line). The background colour of each subplot represents the convective regime (or transition between different convective regimes due to MCP): (dark orange): mobile, (light orange): transition from early-mobility to mobile, (white): transition from early-mobility to episodic, (light green): transition from stagnant to episodic, and (dark green): stagnant.

billion years of the evolution of the models. Showing the average values is interesting because it shows very clearly the tectonic state of the planet, i.e., for the same reference viscosity, smaller lid thickness or internal temperature point to the mobile/episodic-lid regime, while higher values point to the stagnant-lid regime. Lines with different colours connect points with the same reference viscosity in order to help visualising variations caused by different yield stresses.
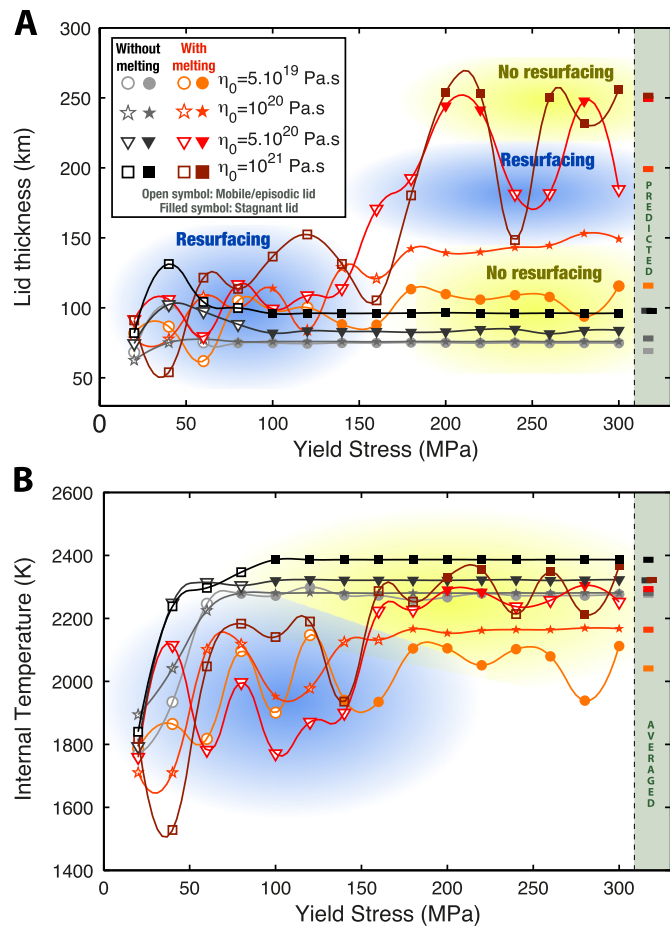
Fig. 4. Values averaged over the last half billion years of the evolution of the models for (A) lid thicknesses and (B) planetary internal temperatures averaged over 200 km below the lithosphere for each case. Different colours and symbols represent different reference viscosities and the use or not of MCP (see legend in the figure for more details). The green patches on the right depict predictions for the lid thickness and average internal temperature values concerning only stagnant-lid cases.

The first and most important observation in Fig. 4(A) is that MCP leads to the formation of a thicker lid. Cases without MCP have lid thicknesses that are very similar for the same reference viscosity even if the yield stress is different, mainly because most of the cases are in a stagnant-lid regime, therefore the cases with some (small) variations are the cases with some mobility. The lid thickness increases as the reference viscosity increases, which is an expected behaviour (see Eq. (6)). When considering MCP, the thickness of the lid can be very different from case to case. The randomness in the lid thickness arises from MCP itself. Compositional heterogeneities are created in the lid due to laterally varying internal convection patterns. This laterally-heterogeneous crust can break the lithosphere more easily, favouring the mobility of the lid. In some cases the lid resurfaces while in others it does not, and looking at Fig. 4(A) it is clear which cases have a stagnant lid, and which cases have a mobile or episodic lid.

4.1.2. Internal temperature

In Fig. 4(B) the interior temperatures averaged over the 200 km below the lithosphere and the last half billion years of evolution are plotted. As expected, models with no lid mobility have higher internal temperatures. Interestingly, cases with MCP have lower internal temperatures; therefore melting combined with magmatism seems to be a very efficient heat loss mechanism, buffering the planetary temperature. This result is in agreement
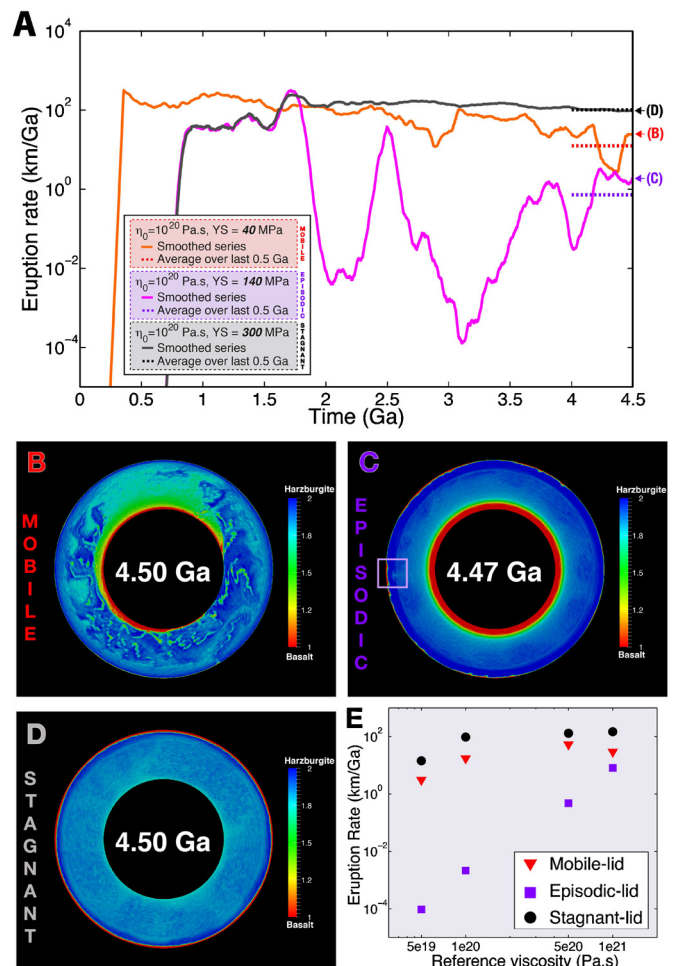

Fig. 5. Eruption rate analysis: (A) Time evolution of eruption rate for three cases with the same reference viscosity, 10^{20} Pa·s, and three different yield stresses (YS), 40 (orange–red), 140 (magenta–purple) and 300 MPa (grey–black). For each case a smoothed time series (solid line) and the average value for the last half billion years (dashed line) are presented. (See legend in the figure for more details.) (B) Composition field for the last stage of the case with YS = 40 MPa. (C) Composition field for the (almost) last stage of the case with YS = 140 MPa. The lilac square encircles a burst of erupting activity forming oceanic crust at the surface. (D) Composition field for the last stage of the case with YS = 300 MPa. (E) Averaged eruption rates for the different reference viscosities used during the last half billion years of evolution, and separated for mobile-, episodic- and stagnant-lid cases, as defined in Fig. 1, but obviously only considering the cases with MCP. Values are shown also in Table 3.

with previous studies (Xie and Tackley, 2004; Keller and Tackley, 2009; Ogawa and Yanagisawa, 2011; Armann and Tackley, 2012; Nakagawa and Tackley, 2012).

4.1.3. Eruption rate

Fig. 5(A) shows the eruption rate throughout time for three cases with identical reference viscosity, 10^{20} Pa·s, and three different yield stresses. The first case (orange–red) has a yield stress of 40 MPa and is a mobile lid case. The eruption rate has no big fluctuations but slowly decreases in time as the material gets more depleted. Fig. 5(B) shows the final composition field for this case, in which we can see a thin subducting basaltic crust and a heterogeneously mixed interior, with some areas where the material is quite depleted and some other areas where the material is relatively enriched. The second case shown in Fig. 5(A) (magenta–purple) has a yield stress of 140 MPa and is an episodic-lid case. In this case the eruption rate displays large fluctuations in time, which are related to lid overturns. These overturns quickly deplete the mantle, which decreases the final eruption rate. The (almost)

final composition field (Fig. 5(C)) for this case displays a very depleted interior with accumulation of a stable basaltic layer at the core–mantle boundary. We choose to show the composition field at 4.47 Ga in order to show the eruption behaviour with strongly depleted material. The lilac square encircles a burst of erupting activity forming oceanic crust at the surface. It appears that the cause of melting is an upwelling from the lower mantle. Finally, in the third case with a yield stress of 300 MPa (represented in grey–black) and in a stagnant-lid regime, crustal production, compared with the mobile-lid case, starts later and is smaller for the early evolution of the planet but then after some time it becomes higher and almost constant with time, leading to a higher average eruption rate than in the other cases. In the final stage of this stagnant-lid case in Fig. 5(C) the interior is well mixed and the material is not as depleted as for example the episodic-lid case. Fig. 5(E) summarises these differences by showing the final (last 0.5 Ga of the evolution) averaged eruption rates for the different reference viscosities used, separated for mobile-, episodic- and stagnant-lid cases, as defined previously. We can clearly see that the final average eruption rate for a stagnant lid is higher than for mobile lid, which in turn is higher than for episodic-lid cases. Finally, eruption rates are higher for higher reference viscosities, but seem to stabilise, becoming similar for the highest reference viscosities. Remarkably, an episodic-lid regime can decrease the final eruption rate by up to 5 orders of magnitude.

4.2. Scaling analysis

4.2.1. Lithospheric critical yield stress without MCP

Heat flux, stresses and internal temperature fields in the stagnant-lid regime have been extensively studied during the last decades (Fowler, 1985; Reese et al., 1998; Solomatov and Moresi, 2000; Solomatov, 2004). It has been shown that the lithospheric stresses generated by mantle thermal convection can be modelled using various scaling laws, all of them involving the internal Rayleigh number, Ra_i, and rheological parameters such as the activation energy and volume (Fowler, 1985; Solomatov, 2004). The internal Rayleigh number is based, among other physical parameters considered, on the internal viscosity, which is itself based on the temperature of the upper mantle, T_i.

In this study we use the observed internal temperature to define the Frank-Kamenestkii parameter, which quantifies how temperature-dependent the viscosity is:

$$\theta = \frac{\Delta T(E_{ol} + P_{UM}V_{ol})}{RT_i^2},$$ (5)

where ΔT is the non-adiabatic temperature difference between the core–mantle boundary and the surface, obtained at the end of the simulations (see Table 3), and P_{UM} is a pressure typically reached in the upper mantle (we use $P_{UM} = 30$ GPa).

In thermal convection models in the stagnant-lid regime, an analytical equilibrium lithosphere thickness δ_a can be calculated using:

$$\delta_a \simeq \frac{hT_i}{Nu\Delta T},$$ (6)

where h is the thickness of the mantle and Nu is the Nusselt number (dimensionless heat flux). In the stagnant-lid regime, the Nusselt number is usually considered to follow Solomatov (1995):

$$Nu \propto Ra_i^{\xi}\theta^{-\gamma},$$ (7)

where ξ and γ are dimensionless positive constants depending on the stationarity of convection and the type of rheology considered. Ra_i is the internal Rayleigh number, defined as:

$$Ra_i = \frac{\alpha\rho g\Delta Th^3}{\kappa\eta_i},$$ (8)

Table 3

For the different reference viscosities η_0 (Pa·s), the first two tables present several averaged (over the last 500 Myrs) and predicted quantities concerning only the stagnant-lid cases: calculated internal temperature T_i (K), observed lithosphere thickness δ (km), predicted lithosphere thickness δ_a (km), calculated temperature gradient at the bottom of the lithosphere $\frac{\partial T}{\partial z}\big|_{obs}$ (K/km) and predicted critical yield stress τ_{ya} (MPa). The third table shows the eruption rates (km/Ga) averaged over the last 500 Ma for the three convection regimes, mobile-, episodic- and stagnant-lid. The ΔT column represents the non-adiabatic top–bottom temperature difference obtained in the end of the simulations.

No melting					
η_0	T_i	δ	δ_a	$\frac{\partial T}{\partial z}\big|_{obs}$	τ_{ya}
$5\cdot 10^{19}$	2275	74.8	69.1	16.1	46.97
10^{20}	2281	75.8	78.1	16.0	55.00
$5\cdot 10^{20}$	2321	83.2	97.8	15.5	78.56
10^{21}	2386	96.1	97.7	13.7	90.08

Melting					
η_0	T_i	δ	δ_a	$\frac{\partial T}{\partial z}\big|_{obs}$	τ_{ya}
$5\cdot 10^{19}$	2041	103.4	115.82	12.0	130.13
10^{20}	2164	144.4	199.08	9.2	233.44
$5\cdot 10^{20}$	2293	244.4	249.20	8.5	313.95
10^{21}	2322	249.0	251.51	8.7	329.44

Erupt. R.				
η_0	Mob.	Epis.	Stag.	ΔT
$5\cdot 10^{19}$	3.1	$9.5\cdot 10^{-5}$	14.3	2492
10^{20}	17.4	$2.1\cdot 10^{-3}$	96.3	2525
$5\cdot 10^{20}$	53.2	$4.8\cdot 10^{-1}$	130.4	2600
10^{21}	29.6	8.1	148.0	2633

where α is the thermal expansivity, ρ is the density, g is the gravitational acceleration, κ is the thermal conductivity and η_i is the internal viscosity (see Table 1 for dimensional values). The internal viscosity is based on the internal temperature and on the pressure P_{UM}. Eq. (7) represents an equilibrium state. However, in our case, both bottom temperature and internal heating are time-dependent. Moreover, it is unclear whether we should use lower mantle or higher mantle viscosity, which may follow a slightly different trend because of adiabatic temperature increase and non-zero activation volume, to define the internal Rayleigh number.

We found that a scaling for Newtonian stationary convection (Fowler, 1985; Reese et al., 1998) satisfyingly represents our lithospheric thickness (δ_a): $Nu = 7.7Ra_i^{1/5}\theta^{-1}$. Our cases are, however, insufficient in number to make an adequate inversion of the coefficients ξ and γ.

Solomatov (2004) gives a scaling law for lithosphere stresses τ_l in the stagnant-lid regime based on the rheological conditions at the bottom of the lithosphere and on the internal activity of the mantle. Considering a visco-plastic upper boundary layer, Solomatov (2004) obtained an analytical formulation for the critical yield stress τ_{ya}, the stress below which a stagnant-lid regime is no longer stable:

$$\tau_{ya} = 13\frac{\alpha\rho g}{\Delta T}\left(\frac{RT_i^2}{E}\right)^2 l_{hor},$$ (9)

where l_{hor} is the average plume spacing in the mantle, given by the expression:

$$l_{hor} = 6.3hRa_{lm}^{-1/4}\theta^{1/4}.$$ (10)

Ra_{lm} is the lower mantle Rayleigh number, which is based on the viscosity at 2400 km depth and on the lower mantle temperature T_{lm}. We do not use the upper mantle Rayleigh number Ra_i here, because lower mantle conditions impose the plume spacing in the absence of subduction zones. For simplicity, we defined the lower mantle temperature using an approximation of the adiabatic temperature increase: $T_{lm} = T_i + 830$. The critical yield stress values (τ_{ya}) calculated for the case without MCP and for the different

reference viscosities are shown in Table 3 and plotted in Fig. 1(A) as the tick dashed blue line. One can see that the predicted critical yield stress calculated from Eq. (9) nicely reproduces the boundary between the cases with some (or a lot of) surface mobility and the cases in a stagnant-lid regime.

4.2.2. Lithospheric critical yield stress with MCP

The comparison between cases with and without MCP is difficult due to the time-dependence of cooling and melting related processes. An equilibrium situation, where elegant scaling laws can be derived, is never reached because of the cooling of the core and the increase of mantle depletion with time. Therefore, we chose to use scaling laws for lid stresses based on the purely thermal convection problem, considering that our system quickly reaches a quasi-equilibrium.

As previously stated, including MCP results in a significantly thicker lid for the cases not in mobile lid regime. One could argue that this increase in lithospheric thickness is only due to the decrease in internal temperature, which is also an effect of MCP (Fig. 4). The decrease in internal temperature leads to an increase in the viscosity, weakening in turn the vigour of convection (cf. Eq. (7)). However, our tests show that the equilibrium Nusselt numbers that one can compute with Eq. (7) are very similar in all stagnant-lid cases considering MCP, even if the reference viscosities span almost two orders of magnitude. This result is due to the variations of internal temperature shown in Fig. 4 – cases with a higher reference viscosity become hotter reducing the internal viscosity. Classical boundary layer theory must be upgraded to explicitly take into account the effects of MCP, in order to predict as accurately as possible lithospheric thicknesses.

In our models, when melting is considered, a significant amount of magma erupts to the surface, where it cools down to surface temperature. For simplicity it is assumed that the percolation of melt through the solid is much faster than convection and thus shallow melt is instantly removed and deposited at the surface to form oceanic crust.

The thickness of the lithosphere can then be obtained by computing the competition between the deposition of new oceanic crust and lithosphere thinning by convective removal of the bottom of the constantly growing lithosphere. Following this, we solve the heat equation in 1D with an imposed down-going velocity, which is constant but inhomogeneous with depth. A similar procedure has been applied before to Io (O'Reilly and Davies, 1981). We, however, use a slightly different approach by imposing the heat gradient at the bottom of the lithosphere according to our numerical simulations results, as a proxy for convective heat flux forcing.

Assuming that the lithospheric thickness is in equilibrium, the heat equation is:

$$\frac{\partial T}{\partial t} = \kappa \frac{\partial^2 T}{\partial z^2} - v \frac{\partial T}{\partial z} = 0, \tag{11}$$

where v is the vertical depth-dependent down-going velocity and z is depth. By using this 1D equation we neglect internal heating (which is not composition-dependent in our case) and lateral density anomalies generated by the inhomogeneous crustal deposition patterns (this will be considered later in the model for the lithospheric critical stress). Moreover, we average the MCP. Since convection erodes the bottom of the lithosphere, the lithospheric down-going velocity v strongly diminishes at the lithosphere-asthenosphere boundary. Therefore, we impose a velocity field that decreases with depth:

$$v = V_{er} \frac{z_0}{z + z_0}, \tag{12}$$

where V_{er} is an eruption velocity based on the averaged eruption rate for the different reference viscosities recorded from our simulations and presented in Fig. 5(E) and Table 3. z_0 is a positive

constant to be determined and that ensures a finite velocity at the surface. We assume a temperature field consistent with equations (11) and (12), of the form:

$$T(z) = T_0 + A(z + z_0)^2, \tag{13}$$

where T_0 and A are positive constants to be determined. Using equations (11), (12) and (13) we obtain that $z_0 = \kappa / V_{er}$. To obtain the analytical thickness of the lithosphere, δ_a, we consider $T(z = \delta_a) = T_\delta$, $T(z = 0) = T_s$ and we impose the bottom temperature gradient as:

$$\frac{\partial T}{\partial z}\bigg|_{obs} = \frac{\partial}{\partial z} T(z = \delta), \tag{14}$$

where $\frac{\partial T}{\partial z}|_{obs}$ is the observed temperature gradient at the bottom of the lithosphere in our numerical simulations. T_δ is the temperature at the bottom of the lithosphere, inside the last deformable layer, such that $\eta(T_\delta) = 100\,\eta(T_i)$, which implies that:

$$T_\delta = \left(\frac{1}{T_i} + \frac{R}{E + pV} \ln 100 \right)^{-1}. \tag{15}$$

The temperature gradient $\frac{\partial T}{\partial z}|_{obs}$ is computed at the depth at which $T = T_\delta$. After some mathematics, we obtain:

$$A = \frac{T_s - T_\delta + \left[(T_\delta - T_s)^2 + (\kappa / V_{er})^2 \frac{\partial T}{\partial z}|_{obs}^2 \right]^{1/2}}{2(\kappa / V_{er})^2}, \tag{16}$$

$$T_0 = T_s - A \left(\frac{\kappa}{V_{er}} \right)^2, \tag{17}$$

which leads to an analytical expression for the lithosphere thickness:

$$\delta_a = \frac{1}{2A} \frac{\partial T}{\partial z}\bigg|_{obs} - \frac{\kappa}{V_{er}}. \tag{18}$$

Fig. 4(A) shows the predicted lithosphere thicknesses, δ_a, for the different cases on the right side, using the same colour code as for the data points. It appears that our first-order model predicts our obtained results very well.

The next step is to find a scaling law for the lithospheric stresses corresponding to the lithosphere thicknesses, δ_a, calculated with Eq. (18). Solomatov (2004) showed that the stress state of the lithosphere depends mainly on the internal mantle activity (either the density anomalies carried by plumes or the activity of the bottom of the lithosphere), and not on the lithospheric thickness. However, in our simulations, the basaltic crust produced by upper mantle melting confers an additional load to the lithosphere. Since the loading of the lithosphere follows the geometry of the upwellings in the upper mantle, the distribution of basalt in the lid is heterogeneous. The density variations between basalt and harzburgite at various depths have to be carefully considered. Above the eclogite phase transition, which is 60 km on Earth, basalt is significantly lighter than harzburgite and tends to form an homogeneously distributed layer around the surface. Therefore, additional stresses above 60 km are negligible. However, below 60 km, basalt transforms into eclogite, which is around 200 kg/m³ denser than harzburgite (Irifune and Ringwood, 1993; Ono et al., 2001). Therefore, when basalt erupts to the surface, the basalt pushed down to depths below that of the eclogite phase transition becomes gravitationally unstable, even if it remains in the lithosphere because of its large viscosity. Due to this, we consider the lithospheric basalt density difference below the eclogite phase transition as an additional source of stresses to Eq. (9), which gives:

$$\tau_{ya} = 13 \frac{\alpha \rho g}{\Delta T} \left(\frac{R T_i^2}{E} \right)^2 l_{hor} + \frac{\Delta \rho g (1.2 \delta_a - D_{ecl})}{2}, \tag{19}$$

where $\Delta\rho$ is the density difference of the basalt compared to the depleted mantle below D_{ecl}, which is the depth of the phase transition to eclogite (60 km on Earth). We use a value of 200 kg/m^3 for $\Delta\rho$, based on mineral physics studies (Irifune and Ringwood, 1993; Ono et al., 2001). The second term on the right hand side of Eq. (19) is divided by 2 to simply take into account the fact that parts of the lithosphere remain at the initial composition. The term 1.2 times the lid thickness accounts for the bottom part of the lithosphere, between T_δ and T_i, which also carries density anomalies. The second term of the right-hand side of Eq. (19) is based only on simple dimensional considerations, however we can see that it is sufficient to accurately represent the boundary between the mobile-/episodic- to stagnant-lid regime when MCP is taken into consideration, as shown in Fig. 1(B) as the thick dashed red curve.

Perhaps a more universal generalisation for the effects of MCP could be found by carefully observing the crustal thickness patterns. However, our first-order approximation seems to explain very well the increase of the critical yield stress for the cases considering MCP.

We stated before that when we look at Fig. 1 we see that the transition from a stagnant lid to an episodic lid due to MCP is not continuous. Combining this and the predicted boundary drawn using Eq. (19), it is interesting to see that the mixed parameter space where both episodic and stagnant lid were obtained is located on the left of the predicted critical stress curve (the dashed area we name "Stagnant (potentially unstable)"). This suggests that fast resurfacing of the lid depends on the fluctuations of the local lithospheric stresses or eruption through time. For example, looking at the first image (at 2.332 Ga) in the sequence showing an overturn in Fig. 2(C), we can see that the occurrence of resurfacing is linked to the activity of the upper mantle. The stationarity of the upper-mantle convection cells can be directly linked to the distribution of basalt (and therefore stresses) in the overlying lithosphere. One expects that stationary upper-mantle cells lead to an heterogeneous distribution of basaltic crust in the lithosphere, resulting in large density contrasts, and consequently increased resurfacing probability. This seems to be consistent with the fact that higher reference viscosity simulations ($\eta_0 = 5 \cdot 10^{20}$ and 10^{21} Pa·s), which are expected to be more stationary than lower viscosity simulations, experience resurfacing for higher yield stress. Interestingly, this is always below the critical yield stress predicted by our simple dimensional scaling (Eq. (19)).

5. Conclusions

Convection regimes obtained in numerical simulations with and without including MCP differ greatly, the main effect being that MCP strongly helps the mobility of the lid. Further effects of MCP in the evolution of a planet are the formation of a thicker lid and lower internal temperatures. Despite the fact that the treatment of MCP used in the present study is a first-order approximation, the effect it has on plate tectonics can be captured: it strongly increases the mobility of the lid, meaning that Earth-like plate tectonics is more likely to occur in planets that have the basic mechanism of producing a crust of variable thickness and different density. Several factors seem to play a role on this, namely heterogeneities in the lid thickness and differences in internal temperature induced by MCP. Based on the observed internal temperature, eruption rate and the temperature gradient at the bottom of the lithosphere, we have shown that the increase of critical yield stress due to MCP can be predicted analytically, due to larger lid thicknesses which generate additional stresses. This is an important result, which may help in explaining the discrepancy in values between the critical stress necessary to yield the stagnant-lid regime in numerical simulations and the expected (higher) values

from laboratory rock deformation experiments. Scalings for lid behaviour based on purely thermal convection are thus not directly applicable to actual planets.

Factors not taken into account in our model, like the effect of the presence of melt in the viscosity of the mush (Zimmerman and Kohlstedt, 2004; Scott and Kohlstedt, 2006) or the presence of water, might influence the results. For example, the findings of Hirth and Kohlstedt (1996) suggest that mantle melting dehydrates and stiffens the shallow part of the mantle, which would help lid stagnation. Also, in our study we consider that all the magmatism is extrusive, however this is not the case in the Earth (Cawood et al., 2013) as intrusive magmatism can play a role in the dynamics of the lithosphere.

Acknowledgements

Appendix A. Supplementary material

Supplementary material related to this article can be found online at http://dx.doi.org/10.1016/j.epsl.2016.01.024.

References

Ammann, M.W., Brodholt, J.P., Wookey, J., Dobson, D.P., 2010. First-principles constraints on diffusion in lower-mantle minerals and a weak D'' layer. Nature 465 (7297), 462–465.

Armann, M., Tackley, P.J., 2012. Simulating the thermochemical magmatic and tectonic evolution of Venus's mantle and lithosphere: two-dimensional models. J. Geophys. Res. 117 (E12), E12003.

Buffett, B.A., Huppert, H.E., Lister, J.R., Woods, A.W., 1992. Analytical model for solidification of the Earth's core. Nature 356 (6367), 329–331.

Buffett, B.A., Huppert, H.E., Lister, J.R., Woods, A.W., 1996. On the thermal evolution of the Earth's core. J. Geophys. Res. 101 (B4), 7989–8006.

Cawood, P.A., Hawkesworth, C.J., Dhuime, B., 2013. The continental record and the generation of continental crust. Geol. Soc. Am. Bull. 125 (1–2), 14–32.

Čížková, H., van den Berg, A.P., Spakman, W., Matyska, C., 2012. The viscosity of Earth's lower mantle inferred from sinking speed of subducted lithosphere. Phys. Earth Planet. Inter. 200–201, 56–62.

Condomines, M., Hemond, Ch., Allègre, C.J., 1988. U–Th–Ra radioactive disequilibria and magmatic processes. Earth Planet. Sci. Lett. 90 (3), 243–262.

Crameri, F., Schmeling, H., Golabek, G.J., Duretz, T., Orendt, R., Buiter, S.J.H., May, D.A., Kaus, B., Gerya, T.V., Tackley, P.J., 2012. A comparison of numerical surface topography calculations in geodynamic modelling: an evaluation of the 'sticky air' method. Geophys. J. Int. 189, 38–54.

Davies, G.F., 2007. Thermal evolution of the mantle. In: Davies, G.F. (Ed.), Treatise on Geophysics. Elsevier B. V., Amsterdam, pp. 197–216.

Dymkova, D., Gerya, T., 2013. Porous fluid flow enables oceanic subduction initiation on Earth. Geophys. Res. Lett. 40 (21), 5671–5676.

Faul, U.H., Jackson, I., 2007. Diffusion creep of dry, melt-free olivine. J. Geophys. Res. 112. B4.

Fowler, A.C., 1985. Fast thermoviscous convection. Stud. Appl. Math. 72, 189–219.

Fowler, A.C., 1993. Boundary layer theory and subduction. J. Geophys. Res. 98 (B12), 21997–22005.

Hernlund, J.W., Tackley, P.J., 2008. Modeling mantle convection in the spherical annulus. Phys. Earth Planet. Inter. 171 (1–4), 48–54.

Herzberg, C., Raterron, P., Zhang, J., 2000. New experimental observations on the anhydrous solidus for peridotite KLB-1. Geochem. Geophys. Geosyst. 1 (11).

Hirth, G., Kohlstedt, D.L., 1996. Water in the oceanic upper mantle: implications for rheology, melt extraction and the evolution of the lithosphere. Earth Planet. Sci. Lett. 144 (1–2), 93–108.

Hofmann, A.W., 1997. Mantle geochemistry: the message from oceanic volcanism. Nature 385 (6613), 219–229.

Hunt, S.A., Weidner, D.J., Li, L., Wang, L., Walte, N.P., Brodholt, J.P., Dobson, D.P., 2009. Weakening of calcium iridate during its transformation from perovskite to post-perovskite. Nat. Geosci. 2, 794–797.

Irifune, T., Ringwood, A.E., 1993. Phase transformations in subducted oceanic crust and buoyancy relationships at depths of 600–800 km in the mantle. Earth Planet. Sci. Lett. 117 (1–2), 101–110.

Karato, S.I., Wu, P., 1993. Rheology of the upper mantle: a synthesis. Science 260 (5109), 771–778.

Keller, T., Tackley, P.J., 2009. Towards self-consistent modeling of the martian dichotomy: the influence of one-ridge convection on crustal thickness distribution. Icarus 202 (2), 429–443.

Kohlstedt, D.L., Evans, B., Mackwell, S.J., 1995. Strength of the lithosphere: constraints imposed by laboratory experiments. J. Geophys. Res. 100 (B9), 17587–17602.

Korenaga, J., Karato, S.-I., 2008. A new analysis of experimental data on olivine rheology. J. Geophys. Res. 113 (B2), B02403.

Lenardic, A., Crowley, J.W., 2012. On the notion of well-defined tectonic regimes for terrestrial planets in this solar system and others. Astrophys. J. 755 (132), 11.

McKenzie, D., Bickle, M.J., 1988. The volume and composition of melt generated by extension of the lithosphere. J. Petrol. 29 (3), 625–679.

Moresi, L., Solomatov, V., 1998. Mantle convection with a brittle lithosphere: thoughts on the global tectonic styles of the Earth and Venus. Geophys. J. Int. 133 (3), 669–682.

Nakagawa, T., Tackley, P.J., 2004. Effects of thermo-chemical mantle convection on the thermal evolution of the Earth's core. Earth Planet. Sci. Lett. 220 (1–2), 107–119.

Nakagawa, T., Tackley, P.J., 2012. Influence of magmatism on mantle cooling, surface heat flow and Urey ratio. Earth Planet. Sci. Lett. 329–330, 1–10.

Nakagawa, T., Tackley, P.J., Deschamps, F., Connolly, J.A.D., 2010. The influence of MORB and harzburgite composition on thermo-chemical mantle convection in a 3-D spherical shell with self-consistently calculated mineral physics. Earth Planet. Sci. Lett. 296 (3–4), 403–412.

Ogawa, M., Yanagisawa, T., 2011. Numerical models of Martian mantle evolution induced by magmatism and solid-state convection beneath stagnant lithosphere. J. Geophys. Res. 116 (E8), E08008.

Ono, S., Ito, E., Katsura, T., 2001. Mineralogy of subducted basaltic crust (MORB) from 25 to 37 GPa, and chemical heterogeneity of the lower mantle. Earth Planet. Sci. Lett. 190 (1–2), 57–63.

O'Reilly, T.C., Davies, G.F., 1981. Magma transport of heat on Io: a mechanism allowing a thick lithosphere. Geophys. Res. Lett. 8 (4), 313–316.

Reese, C.C., Solomatov, V.S., Moresi, L.N., 1998. Heat transport efficiency for stagnant lid convection with dislocation viscosity: application to Mars and Venus. J. Geophys. Res. 103 (E6), 13643–13657.

Regenauer-Lieb, K., Yuen, D.A., Branlund, J., 2001. The initiation of subduction: criticality by addition of water? Science 294 (5542), 578–580.

Rolf, T., Tackley, P.J., 2011. Focussing of stress by continents in 3D spherical mantle convection with self-consistent plate tectonics. Geophys. Res. Lett. 38 (18).

Rozel, A., 2012. Impact of grain size on the convection of terrestrial planets. Geochem. Geophys. Geosyst. 13 (10).

Schubert, G., Turcotte, D., Olson, P., 2001. Mantle Convection in the Earth and Planets. Cambridge University Press, Cambridge.

Scott, T., Kohlstedt, D.L., 2006. The effect of large melt fraction on the deformation behavior of peridotite. Earth Planet. Sci. Lett. 246, 177–187.

Solomatov, V.S., 1995. Scaling of temperature- and stress-dependent viscosity convection. Phys. Fluids 7 (2), 266–274.

Solomatov, V.S., 2004. Initiation of subduction by small-scale convection. J. Geophys. Res. 109. B01412.

Solomatov, V.S., Moresi, L.-N., 2000. Scaling of time-dependent stagnant lid convection: application to small-scale convection on the Earth and other terrestrial planets. J. Geophys. Res. 105, 21795–21818.

Stein, C., Schmalzl, J., Hansen, U., 2004. The effect of rheological parameters on plate behaviour in a self-consistent model of mantle convection. Phys. Earth Planet. Inter. 142, 225–255.

Stevenson, D.J., 1990. Fluid dynamics of core formation. In: Origin of the Earth, pp. 231–249.

Tackley, P.J., 2000. Self-consistent generation of tectonic plates in time-dependent, three-dimensional mantle convection simulations. Geochem. Geophys. Geosyst. 1 (1).

Tackley, P.J., 2008. Modelling compressible mantle convection with large viscosity contrasts in a three-dimensional spherical shell using the yin-yang grid. Phys. Earth Planet. Inter. 171 (1–4), 7–18.

Tackley, P.J., Ammann, M., Brodholt, J.P., Dobson, D.P., Valencia, D., 2013. Mantle dynamics in super-Earths: post-perovskite rheology and self-regulation of viscosity. Icarus 225 (1), 50–61.

Weller, M.B., Lenardic, A., 2012. Hysteresis in mantle convection: plate tectonics systems. Geophys. Res. Lett. 39 (10).

Williams, Q., Garnero, E.J., 1996. Seismic evidence for partial melt at the base of Earth's mantle. Science 273, 1528–1530.

Xie, S., Tackley, P.J., 2004. Evolution of U–Pb and Sm–Nd systems in numerical models of mantle convection and plate tectonics. J. Geophys. Res. 109 (B11), B11204.

Yamazaki, D., Karato, S.-I., 2001. Some mineral physics constraints on the rheology and geothermal structure of Earth's lower mantle. Am. Mineral. 86 (4), 385–391.

Zerr, A., Diegeler, A., Boehler, R., 1998. Solidus of Earth's deep mantle. Science 281 (5374), 243–246.

Zimmerman, M.E., Kohlstedt, D.L., 2004. Rheological properties of partially molten lherzolite. J. Petrol. 45 (2), 275–298.